Preprint
UCRL-JC-145192

Multi-Kilovolt X-Ray Conversion Efficiencies

C. A. Back, J. L. Davis, J. Grun, O. L. Landen, M. C. Miller, L. J. Suter

This article was submitted to
International Symposium on Optical Science and Technology
San Diego, CA
July 29 through August 4, 2001

August 23, 2001

U.S. Department of Energy

Lawrence
Livermore
National
Laboratory

Multi-kilovolt X-ray Conversion Efficiencies

C. A. Back, J. L. Davis[a], J. Grun[b], O. L. Landen, M. C. Miller, L. J. Suter
Lawrence Livermore National Laboratory, L-21, P.O. Box 808, Livermore, CA 94551, [a]Alme & Associates, 6020 Richmond Hwy., Ste 204, Alexandria, VA, [b] Naval Research Laboratory, 4555 Overlook Ave, S.W., Washington, D. C. 20375,

ABSTRACT

X-ray sources in the 3-7 keV energy regime can be produced by laser-irradiating mid- and high-Z gas-filled targets with high-powered lasers. A series of experiments have been performed using underdense targets that are supersonically heated with ~ 35 kJ of 0.35 μm laser light. These targets were cylindrical Be enclosures that were filled with 1-2 atms of Xe or Ar gas. L-shell x-ray emission is emitted from the plasma and detected by Bragg crystal spectrometers and x-ray diodes. Absolute flux measurements show conversion efficiencies of ~ 10% in the multi-kilovolt x-ray emission. These sources can be used as bright x-ray backlighters or for material testing.

Keywords: multi-keV X-ray conversion efficiency, L-shell emission, laser-produced plasma, backlight source

1. INTRODUCTION

Multi-keV x-ray sources can be routinely produced at high-powered laser facilities. In the last ten years, they have been extremely useful in the radiography of high energy density laser-produced plasmas. Now, we are focussing research on the sources themselves to increase conversion efficiency, especially for photon energies greater than 3 keV. These sources are needed to probe higher areal density and higher Z plasmas, such as those that will be created on the National Ignition Facility, and also for new material testing applications.

Recent experiments in which a confined gas is supersonically heated by a laser have shown that > 10% of the energy can be converted into multi-keV x-rays > 3 keV. This is in contrast to radiative sources that are typically produced by irradiating disk or hohlraum targets. For solid disks, the conversion efficiency has been studied as a function of laser intensity, laser wavelength, laser pulse length, and target material. These studies have produced an experimental database of conversion efficiencies.[1-4] Data from many different laboratories show a steep decline in conversion efficiency with photon energy. Overall, the fraction emitted in multi-keV x-rays is < 1%, even though the total conversion efficiency integrated over all photon energies may be significant, especially for higher Z elements.[5]

The important characteristics of x-ray sources include the brightness, frequency distribution, temporal duration, size, and spatial uniformity. In general maximum brightness is always desirable. However, the frequency distribution and temporal duration of any particular source are determined by the application of interest. For inertial confinement fusion (ICF) sources have a near-blackbody frequency distribution, on the order of ns, and can either be constant in intensity, or shaped to optimize implosion trajectories. For radiography, maximum brightness in a limited bandwidth is needed with both long and short duration backlighting applications. In addition, a small source size may be important to minimize spatial blurring of the image in point projection applications. Or, a large uniform source size may be desirable for area backlighters.[6,7]

Material testing and radiography require high flux at hard x-ray energies. The conversion of laser energy into useable x-rays is quantified in conversion efficiency (CE) measurements where the total energy that is emitted by the source in a particular spectral bandwidth is divided by the absorbed laser energy. Many conversion efficiency studies have focussed on

the sub-keV x-ray range.[8-10] Those studies have been motivated by indirect ICF where near local thermodynamic equilibrium (near-LTE) radiation sources drive implosions. For ICF applications, the radiation drive is produced inside of hohlraums, cylindrical or spherical cavities that are irradiated by a laser. The frequency distribution of the source is nearly Planckian, peaking at ~ 2.8 kT and the energy is often characterized by σT^4 where σ is the Stefan-Boltzmann coefficient and T is an effective blackbody radiation temperature. At multi-keV energies, creating blackbody sources with frequency distributions that peak at multi-keV photon energies is difficult even with high-powered lasers. Therefore, x-ray source development for material testing and radiography must concentrate on non-LTE sources.

We have developed an underdense x-ray source that fulfills all of the important characteristics of x-ray sources discussed above.[11] These sources are produced by laser-heating gas-filled targets.[12,13] The gas is filled to a pressure such that the electron density in the plasma, n_e, is less than the critical density of the laser in cm^{-3}, $n_c = 1.1 \times 10^{21} / \lambda_L^2$, where λ_L is the wavelength of the laser in microns. Laser energy is then absorbed through collisional damping of the laser light wave and the heat front propagates supersonically through the target.

The plasma conditions for optimizing multi-keV x-ray emission from gas targets are similar to those required for simple disk targets, however, the method for optimizing these sources is different. The most significant increase in disk conversion efficiency to date was achieved by increased coupling of the laser energy into the target by using a shorter laser wavelength. For gas-filled targets, the initial parameters of the pressure, size, and optimal temperature can all be more easily controlled to produce highly-ionized plasmas that generate copious amounts of multi-keV x-rays. Future gas-filled targets can even employ advanced designs that manipulate the hydrodynamic motion to maximize the emission.

2. MULTI-KILOVOLT CONVERSION EFFICIENCY

The basic advantages of a gas target over a disk target in generating multi-keV x-rays can be shown by one-dimensional calculations. For comparison, the underdense radiator is considered a cylindrical gas column with a diameter equal to that of the laser. In Fig. 1, the temperature and density gradients for an underdense radiator initially at 0.01 g/cc are compared to a denser disk-like target initially at 0.1 g/cc. In both figures, a 0.35 μm wavelength laser with a power of 15 TW is incident from the right onto a target at z=0. Multi-keV emission is typically created in high temperature regions where the heated material becomes highly ionized. For disk-like targets, the density steeply falls as the plasma expands from the surface of the target in the positive z direction. For an underdense radiator where the laser has propagated in ~ 1 mm the amount of plasma with $n_e > 10^{21}$ cm^{-3} and temperatures > 5 keV has significantly increased.

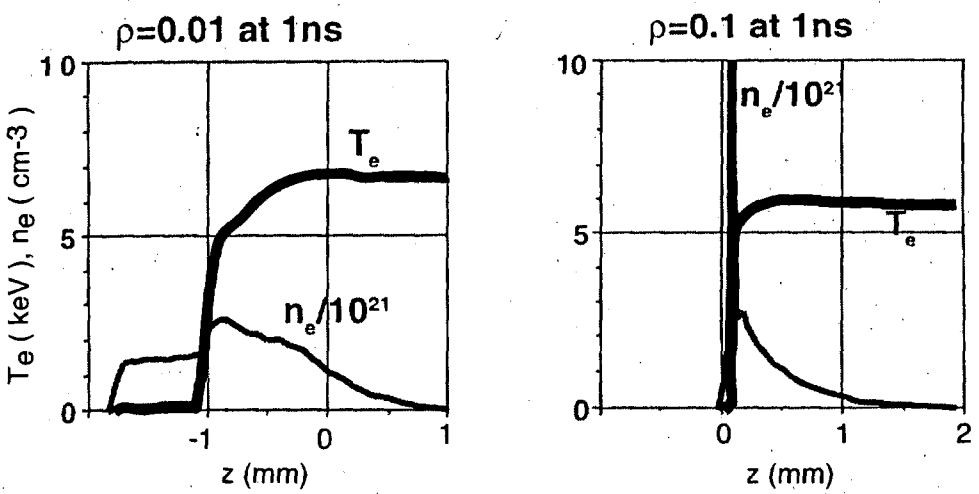

FIGURE 1. Examples of plasma gradients generated in gas targets (left) and solid disk targets (right). These one-dimensional calculations show an increased volume of low density plasma in the gas target which attains temperatures sufficient for producing multi-keV x-rays.

These sources are efficient because an increased volume of plasma at approximately 10^{21} cm^{-3} is created. The absorption length over which energy is deposited is determined by the inverse bremsstrahlung length, ℓ, where Z is the ionic charge (neutral = 0), ln Λ is the Coulomb logarithm, λ_L is the laser wavelength in μm, T_e is the electron temperature in keV, n_e is the electron density in cm^{-3}, and n_c is the critical density in cm^{-3}.[14]

$$\ell = \frac{0.56\,\lambda_L^2\,T_e^{3/2}}{\left(n_e/n_c\right)^2 Z \ln(\Lambda)}\sqrt{1-\left(n_e/n_c\right)} \qquad (1)$$

For Xe-filled targets discussed below, plasma conditions produce an average Z=44, $n_e = 0.1\ n_c$, and $T_e \sim 5$ keV. For a Coulomb logarithm ln Λ = 8, the absorption length is ~ 0.5 mm.

A clearer picture of the energetics of the target is provided by simulations. Figure 2 shows a comparison of the partition of total energy absorbed after 2 ns by a Xe gas target and Ti disk target. It plots the absorbed laser energy partitioned into electron thermal energy, kinetic energy, ion thermal energy, and reradiated energy.

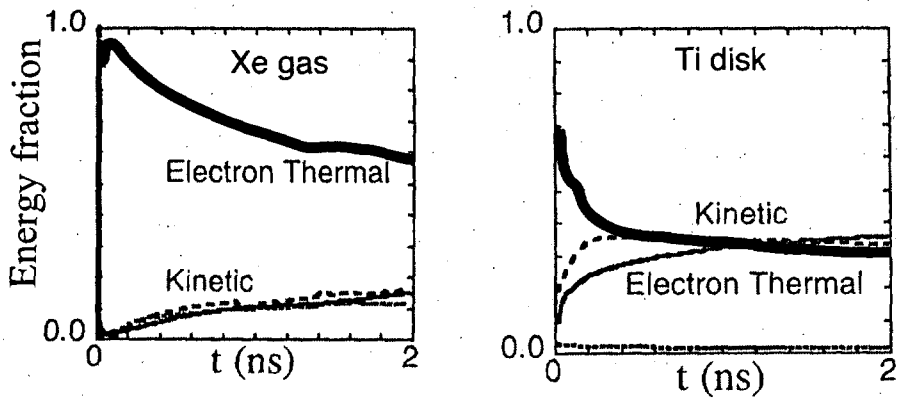

FIGURE 2. The energy balance of a gas-filled target and a traditional solid disk target. Compared to the disk target, the fraction of thermal energy (thick solid line) in the gas-filled target is increased at the expense of the kinetic energy (dotted line). The fraction of total reradiated energy in sub-keV and multi-keV x-rays is shown by the thin solid line.

The kinetic energy is given by $1/2\ m_e v_e^2 + 1/2\ m_i v_i^2$ while the thermal energy of the plasma is $1.5\ n_e kT_e$ and , $1.5\ n_e kT_i$ for the electron or ions, respectively. From these calculations, we find that gas-filled targets are much more efficient at increasing the temperature in the plasma, thereby increasing the thermal energy in the plasma at the expense of the kinetic energy of the plasma. The higher temperature means that more energy is expended ionizing and heating the gas. This leads to an increased fraction of energy reemitted as radiation by these plasmas. Thus the heating of underdense gas-filled targets creates plasma conditions that are more optimized for multi-keV radiators.

Furthermore, the supersonic heating and underdense gas eliminate the ablative subsonic heating that occurs in solid disk targets. The thin solid line in Fig. 2 represents the total radiated energy. Although the total radiated energy is larger in the disk target, this is deceptive since a large fraction is sub-keV x-rays generated in the denser ablative part of the target. The reduction in soft (sub-keV) x-ray emission can be seen in Fig. 3 where the emission as a function of photon energy is plotted for the Xe-gas and a Ti disk.

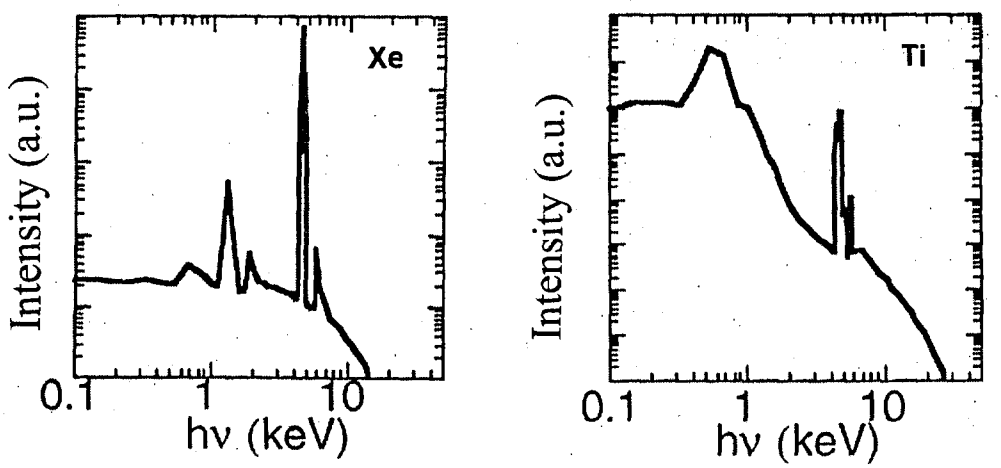

Figure 3. Calculations of the spectra emitted from the gas-filled target and disk x-ray sources. The gas-filled target has a larger fraction of multi-keV x-rays due to the strong L-shell emission of the ionized high-Z gas. The disk target emission peaks in the sub-keV region due to low temperature dense plasma in the conversion layer of the plasma.

The spectra shown in Fig. 3 are calculated using an average atom model. L-shell emission is complex, therefore simplified atomic models are often used in calculating the emission in hydrodynamic simulations. These codes are not spectroscopically accurate. However to first order, the energy balance in the target is insensitive to the photon energies and shell emission involved, so the trend in the relative weightings of the sub-keV and multi-keV energies are meaningful. Calculations of the x-ray using a more detailed atomic model can produce ~ 25 % differences in absolute flux. For the Ti disk, the high density plasma in the conversion layer is primarily heated by conduction and its radiation peaks at 0.6 keV. Calculations of the gas-filled target show that the emission of the L-shell at ~ 4.8 keV dominates the sub-keV emission. Therefore, the fraction of thermal energy in the target, which is associated with the low temperature, sub-keV emission, is smaller. For plasma conditions at 5 keV in the calculations shown below, the plasma can be approximated by a coronal model because its temperature is in the range of 1 to 3 times the ionization energy of the dominant ions in emission, 4.8-5.4 keV for L-shell Xe.[15]

3. EXPERIMENTAL RESULTS

The experiments were performed on the Nova and Omega 0.35 μm wavelength lasers, using either 35.6 ± 3.2 kJ in ten beams delivered in a 2 ns long square pulse or 20 kJ ± 2.0 kJ in forty beams delivered in a 1 ns long square pulse, respectively. Figure 4 shows a schematic of the target and the laser irradiation. Five beams of Nova or 20 beams of Omega entered through laser entrance holes (LEH) from each side of a cylindrical Be enclosure, or "can", containing either Xe or Ar gas. Opposite beams produce overlapping spots on the inside wall.

The cylindrical enclosure was 2 mm in diameter and 1.6 mm long. It was constructed from a 100 μm thick Be tube, capped on either end by 50 μm thick Be washers. The holes in the washers were 1.5 mm in diameter and covered with 3500 Å of polyimide ($C_{16}H_6N_2O_4$) to confine the gas. The low Z beryllium transmits x-ray energies > 2 keV through its walls.

The enclosure itself was designed to have two functions: 1) to serve as a pressure vessel to contain the gas, and 2) to provide hydrodynamic tamping of the gas so the target does not disassemble like gas-filled balloons, so-called "gas bags", used in other plasma studies.

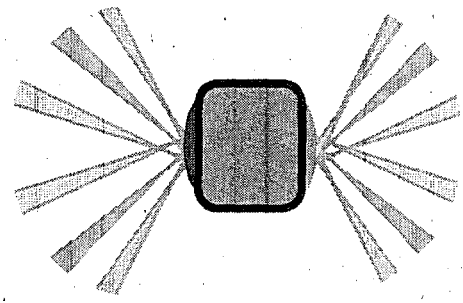

FIGURE 4. Schematic of a gas-filled Be enclosure. Laser beams enter through two holes in the endcaps and heat either Xe or Ar gas. Thin polyimide membranes confine the gas inside and can withstand pressures of ~ 2 atm.

The laser beams were focussed so that the expanding beams directly irradiated as large a volume of gas as possible. Laser absorption within the gas takes place predominantely by inverse bremsstrahlung at densities less than n_c. In addition, best focus was placed outside the enclosure to keep beam intensities lower and thus help reduce possible backscatter of the laser light[17]. The intensity varies from 2 x 10^{15} W/cm ^{2} at the LEH to 4 x 10^{14} W/cm^2 at the wall of the Be cylinder. The pathlength through the gas was 1.3 mm long from the LEH to the wall.

The targets had gas fills of 80% Xe and 20 % Kr, or 100% Ar. The primary gas of interest in the first case is the Xe; the Kr was added to act as a K-shell spectroscopic tracer.[4] In simulations, the presence of the tracer did not affect the hydrodynamics. Experimentally, x-ray images and CE data from supporting shots did not show evidence that the tracer perturbed the plasma. The initial density of the plasma is measured with high accuracy by transducers which monitor the gas pressure. When ionized to a charge state of 44, the nominal 1 atm gas pressure translates to n_e ~1 x 10^{21} cm^{-3}, which is ~ 0.1 n_c. In the Xe experiments initial fill pressures varied from 0.5 to 2.3 atm (~5-25% n_c). For the Ar, we have performed a scan of pressures ranging from 0.5 to 3.0 atm (~2-13% n_c).

A full complement of diagnostics obtained both time-integrated and time-resolved data of the emission. The primary diagnostics included a time-integrated Bragg crystal spectrometer, which provides absolute measurements of the spectra, and x-ray diodes which measure the temporal history of the integrated flux. Two-dimensional x-ray images of the source were also obtained by gated x-ray diagnostics.

The Bragg crystal spectrometers record the spectrally-resolved absolute flux. On each piece of data, we obtain three regions of exposure that are differentially filtered by cold x-ray filters. With different Ti, V, and Al filter attenuations, we are able to cover a dynamic range of ~ 20 to measure the weak and strong line intensities on a single shot. The spectroscopic identification of the Xe lines shows prominent Ne-like n=3-2 and n= 4-2 emission. To obtain conversion efficiency measurements, the time-integrated spectrum is spectrally integrated over the 4-7 keV energy range to obtain the total energy emitted in the L-shell radiation from the plasma with the assumption of isotropic emission. For Ar, the spectrum is integrated from 3-5 keV.

Data is converted from exposure to flux by taking into account the transmission of x-ray filters, the sensitivity of x-ray film, and the Bragg crystal reflectivities. The thin filters were calibrated by spot measurements using a stationary x-ray anode source as well as by checking for self-consistency in the attenuation of different exposure regions. We used the

published calibrations of Henke et al.[18] for DEF x-ray film to convert from exposure to flux. The overall error bar on these measurements is ~ 25 %.

Figure 5 shows an example of the experimental spectra of Xe and Ar measured by the Bragg crystal spectrometer. From the Bragg crystal spectra, we can also experimentally determine T_e. A temperature diagnostic using the Na-like satellite to the Ne-like resonance line of the n = 4-2 transitions has been identified by kinetics modeling of Xe plasmas.[19] The laser heating produces an immediate onset of emission, which monotonically grows and peaks near the end of the pulse. Since equilibration times between the excited states of the ionized Xe are on the order of tens of ps and the gas is supersonically heated, the time-integrated ratio should provide a reasonable temperature measurement. The ratio of these n = 4-2 lines give values between 0.5 and 0.8 which corresponds to an electron temperature range of 4.5 to 5.5 keV. The Kr spectra were also consistent with this temperature range, but spectral dispersion of the ~ 13 keV K-shell lines was not sufficient for a more precise determination.

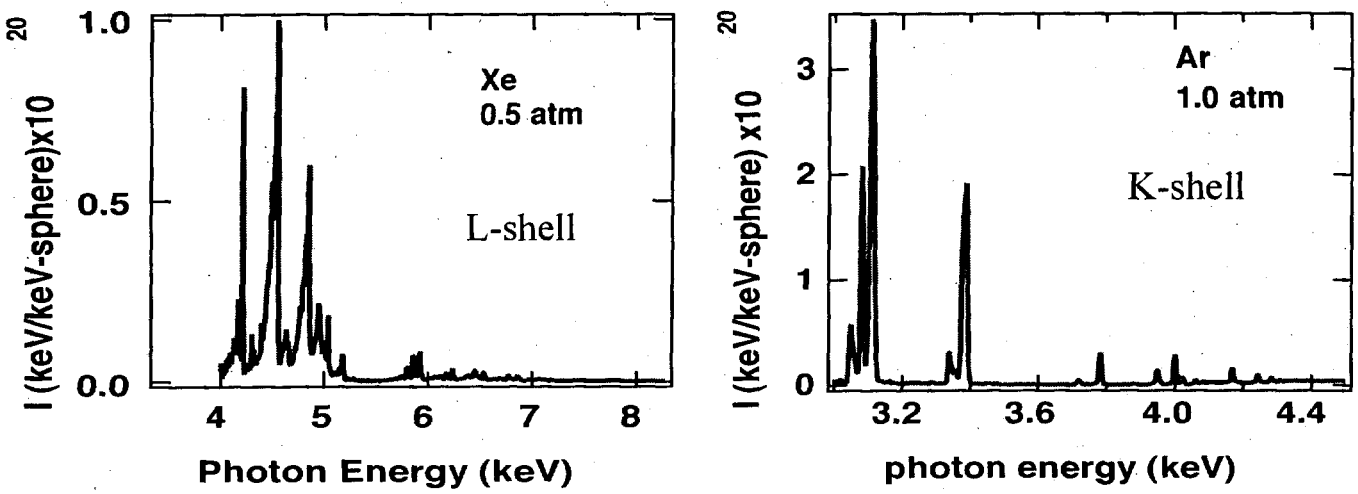

FIGURE 5. Example of the spectrum recorded from the gas-filled Xe and Ar target.

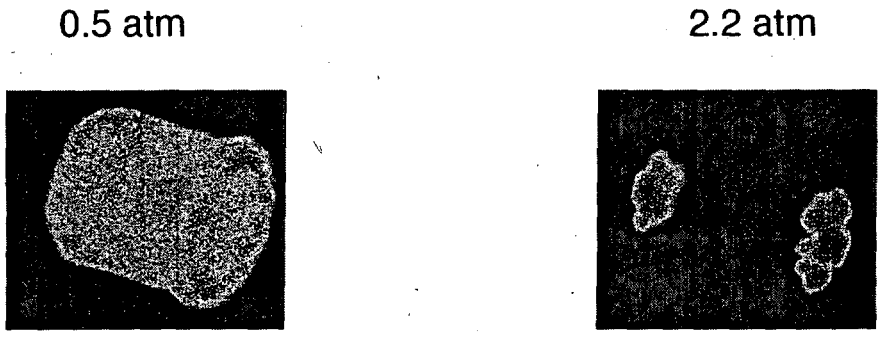

FIGURE 6. Example of x-ray images for Xe emission > 4 keV recorded from a gas-filled target at 0.3 ns after the beginning of a 1 ns laser pulse.

X-ray pinhole cameras provide images of the x-ray source size that are integrated over ~ 80 ps. The bleaching wave formed by the laser creates a high temperature sufficient to ionize Xe and Ar quickly. Emission of the n=4-2 and n=3-2 transitions begin instantaneously and 2-D images show the entire volume emitting 0.3 ns into the 2 ns pulse for photon energies greater than 4 keV. However, due to the density and Z dependence of the inverse bremsstrahlung absorption length, images taken during the beginning of the laser heating of the gas can show a much smaller volume of gas in emission. Simulations predict that targets whose size is optimized to the laser energy and irradiation can absorb approximately 90 % of the laser energy.

Figure 7 shows the CE for different initial gas fill pressures. Both show increasing conversion efficiency with density until approximately 10^{21} cm^{-3}. These conversion efficiencies are roughly an order of magnitude higher than the disk targets. We are currently comparing these results to calculations and find agreement within 25% for pressures up to 1 atm. At higher pressures, calculations predict higher conversion efficiencies than are measured and we are investigating opacity effects which may account for the discrepancies.

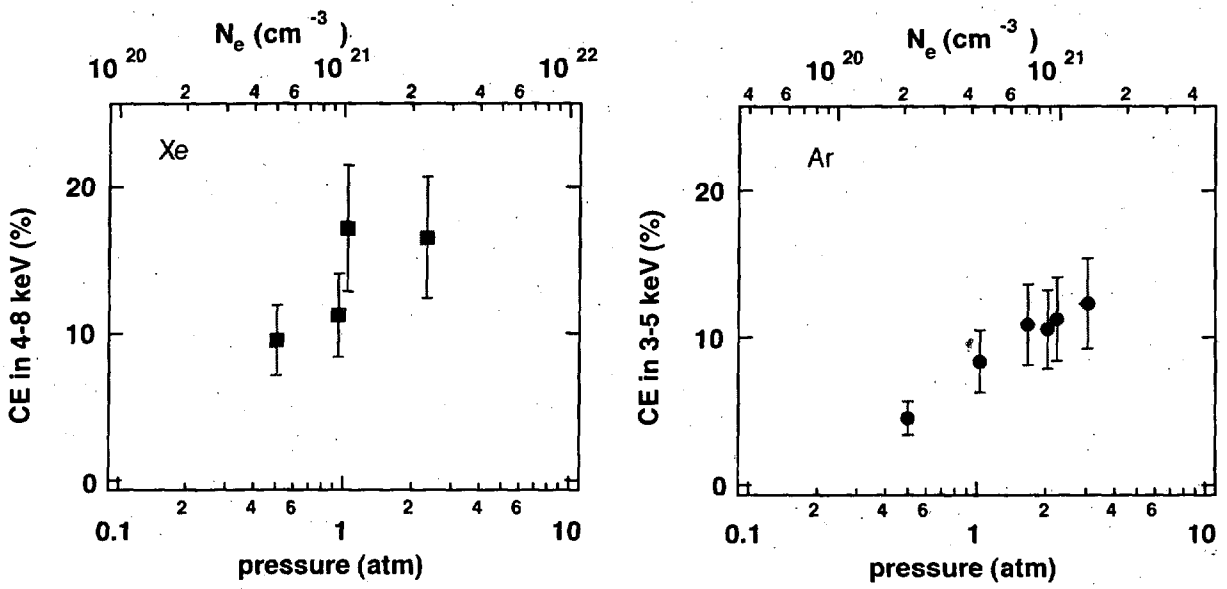

FIGURE 7. The x-ray conversion efficiency from Xe and Ar underdense gas-filled targets. Squares represent Xe and the circles represent Ar.

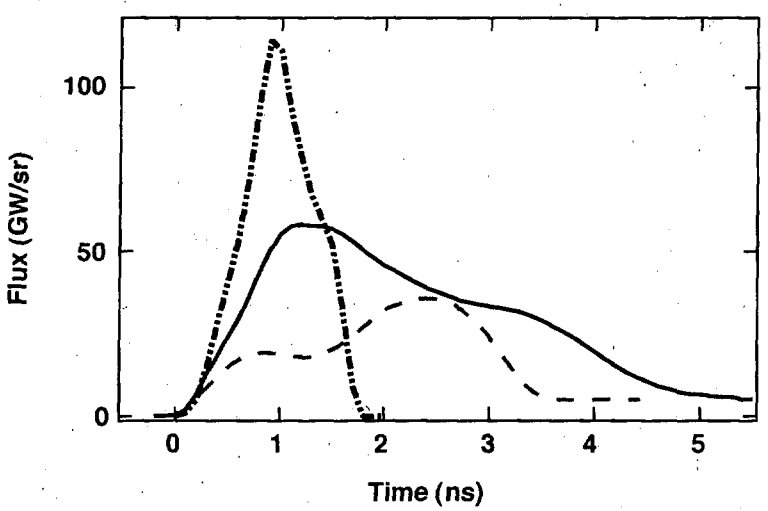

FIGURE 8. The temporal history of the flux from 1 atm Xe (dot-dashed), 2.2 atm Ar (solid), and 1 atm Ar (dashed) underdense gas-filled targets.

Furthermore, the hydrodynamic evolution of the target also affects the absolute emissivity and temporal profile of the multi-keV x-ray conversion efficiency. In Fig. 8 we show some examples of the temporal history of the flux emitted by the different Z gases. The temporal dependence of the x-ray pulse is measured by the filtered x-ray diodes and show a marked dependence on Z and initial density. At all pressures, the Xe tends to increase and peak at the end of the laser pulse. The Ar temporal dependence, however, does not necessarily peak at the end of the laser pulse. In fact, for pressures $\leq$ 1 atm, the peak of the emission occurs after the laser pulse is off. In addition, static pinhole images show bright emission only along the center of the hohlraum axis. Taken together these data indicate that the emission for lower pressure Ar fills are dominated by compression along the axis of stagnation rather than to direct laser heating.

More research will investigate the physical processes in more detail to enable better tailoring of the gas-fill and target sizes. However, since the gas heating is largely governed by the inverse bremsstrahlung absorption, we can develop a scaling which allows us to predict x-ray conversion efficiencies that should be realizable on the National Ignition Facility.

Since the plasma is predominantly heated by a supersonic heat wave, we can consider the plasma model for a gas target discussed by Denavit and Phillion to calculate a scaling for the temperature.[20] As in that paper, we determine the laser energy deposition in a volume defined by the diameter of the laser beam and the inverse bremsstrahlung absorption length, ℓ.[21] We then balance the source heating term due to the laser power (TW) with an electron conduction loss term, which yields:

$$T_e = \left[\frac{\left(n_e/n_c\right)^2}{65\lambda_L^{\,2}} \frac{(Z \ln \Lambda)^2 P_L}{\sqrt{1-\left(n_e/n_c\right)}} \right]^{0.2} \qquad (2)$$

For the experimental conditions, i.e. P_L = 17.8 TW , n_e/n_c = 0.1, and average charge Z of 44, this equation yields a T_e of 4.9 keV. In general, Z is temperature-dependent,[22] but for these plasma conditions it is weakly dependent on T_e and we find good agreement between the measured and calculated time-averaged T_e measurement. Even if the radiative losses were comparable to the conduction losses, T_e would only be a factor of $(1/2)^{0.2}$, or 13% lower. Therefore even though it was derived for low–Z gases , this laser energy deposition model of an idealized plasma column should still provide a reasonable temperature estimate for this high-Z plasma.

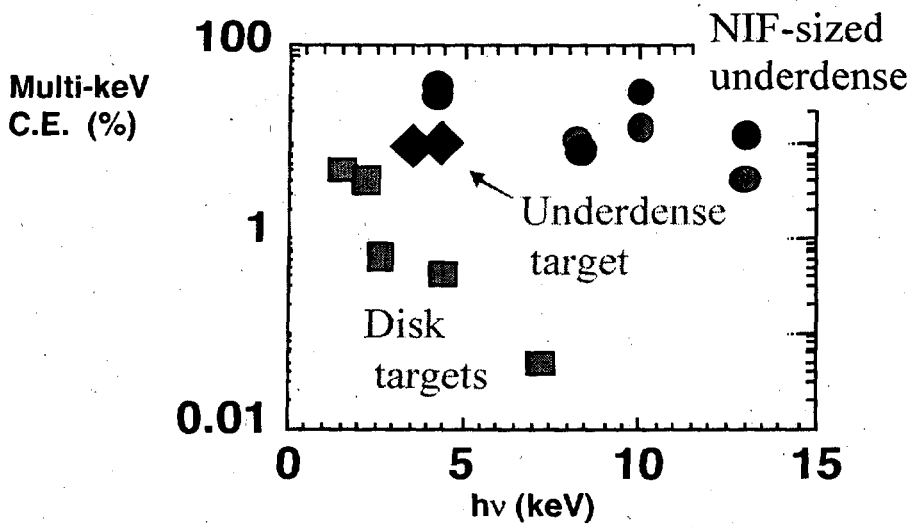

FIGURE 9. Conversion efficiency measured and calculated as a function of intensity for a variety of targets. Squares are disk measurements, diamonds are gas target measurements, and circles are calculations.

Figure 9 shows a summary of the conversion efficiencies of multi-keV x-rays measured by different laboratories. Significant bound-bound emission for x- ray photon energies > 4 keV is generated in K-shell emission for atomic numbers > 20 or in L-shell emission for Z > 53. The conversion efficiency from laser-produced x-ray sources is usually measured in photon energy ranges where bound-bound emission is dominant. Disk target data are represented by squares and show an exponential decline in conversion efficiencies with photon energy. The data from the Ar and Xe gas-filled targets discussed in this paper are shown as diamonds. Also shown in Fig. 9 are extrapolations to facilities such as NIF where up to 500 TW of laser power will be available. The 30x larger NIF power could be distributed to produce 30 modular targets at the same size and the same temperature. Or alternatively, by inspection of Eq. (2), NIF could heat the same size target to 2x higher temperature, and get similar CE at twice the photon energy (e.g. using pre-ablated Ge K-shell emission at 10 keV). Simulations for Cu , Ge, and Kr are shown on the graph by circles for the 60 TW and 300 TW of NIF power, which confirm the simple scaling model (same conversion energy at NIF at twice the photon energy.)

4. CONCLUSIONS

New multi-keV sources have been developed on the Nova and Omega laser facilities. These sources are underdense radiators that take advantage of bound-bound radiation to maximize emission in the 3-7 keV photon range. The method of production is by supersonic heating of a confined gas. This technique allows efficient ionization of high-Z atoms, with less energy expended in kinetic energy and parasitic sub-keV emission losses.

The radiators have well-defined, uniform source size which is advantageous for radiography, material testing, and next-generation fluorescence-type diagnostics. Furthermore, applications of these types of sources can be very diverse. For instance, the targets are modular and for future NIF applications, they can be multiplexed to provide extended sources for irradiating large areas. Or with standardized laser and target conditions, they may become instrument calibration sources.

ACKNOWLEDGEMENTS

The authors would like to thank R. Kauffman, B. Hammel, F. Ze for crystal calibrations, and the Nova and Omega laser and target fabrication crews. This work was performed under the auspices of the U.S. Department of Energy by University of California Lawrence Livermore National Laboratory under contract No. W-7405-Eng-48 and is supported in part by the U. S. DTRA contract number IACRO 98-3064, Work Units 57424 and 57425 and contract MIPR-00-2010/6171 to the Naval Research Laboratory.

REFERENCES

1. Matthews, D. L., Campbell, E. M., Ceglio, N. M., et al., *J. Appl. Phys.* **54**,. 4260 (1983).
2. Phillion, D. and Hailey, C. J., *Phys. Rev. A* **34**, 886 (1986).
3. Kodama, R., Okada, K., Ikeada, N., et al., *J. Appl. Phys.* **59**, 3050 (1986).
4. Yaakobi, B., Bourke, P., McCrory, R., et al, *Opt. Commun.* **38**, 196 (1981).
5. Kauffman, R. L., "X-ray Radiation from Laser Plasma" in *Handbook of Plasma Physics*, vol. 3, eds. Rubenchik and Witkowski, pp. 111-162 (Elsevier Science, North-Holland, 1991) and references therein.
6. Glendinning, S. G., et al., Phys. Plasmas **7**, 2033 (2000);); Ze, F., et al., *J. Appl. Phys.* 66, 1937 (1989).
7. Lindl, J. D., *Phys. of Plasmas* **2**, 3933-4024 (1995) and references therein.
8. Sigel, R., Eidmann, K. Lavarenne, F. and Schmalz, R. F. *Phys. Fluids B* 2, 199 (1989); Eidmann, K., Schmalz, R. F. and Sigel, R. *Phys. Fluids B* **2**, 208 (1989).
9. Mochizuki, T., Yabe, T. , Okada, K., Hamada, M., Ikeda, N., Ikyokama, S. and Yamanaka, C., *Phys. Rev. A* **33**, 525 (1986).
10. Kauffman, R. L., Suter, L. J., Darrow, C. B., Kilkenny, J. D., et al., *Phys. Rev. Lett.* **73**, 2320 (1994).
11. C. A. Back, J. Grun, C. D. Decker, J. L. Davis, O. L. Landen, L. J. Suter, and R. Wallace, " Production of multi-kilovolt X-rays from laser-heated targets", Applications of X Rays Generated from lasers and Other Bright Sources, ed G. A. Kyrala and J-C Gauthier, 3157, 130-137, SPIE, Bellingham, WA (1997).
12. Kauffman, R. L., et al. ICF Quarterly Report 6 (2), 96, Lawrence Livermore National Laboratory, CA UCRL-LR-50021-96-2 (1996).
13. Suter, L. J., Kauffman, R. L., Davis, J. F. and Maxon, M. S., ICF Quarterly Report 6 (3), 96, Lawrence Livermore National Laboratory, CA UCRL-LR-105821-96-3 (1996).

14. Dawson, J. , Kaw, P. , and Green, B. , *Phys. Fluids* **12**, 875 (1969); Lindl, J. *Inertial Confinement Fusion*, Springer-Verlag, New York, 1998, chapter 8 and 11.
15. C. Decker, private communication.
16. R. K. Kirkwood, *et al.*, Phys. Rev. E **77**, 2706 (1996); S. H. Glenzer, C. A. Back, K. G. Estabrook, *et al.* Phys. Rev. E **55**, 927 (1997).
17 .W. Kruer, *The Physics of Laser Plasma Interactions*, (Addison-Wesley, New York, 1988).
18. Henke, B. L., Fujiwara, F. G., Tester, M. A., Dittmore, C. H. and Palmer, M. A., *J. Opt. Soc. Am. B* **1**, 828 (1984).
19. Keane, C. J., Hammel, B. A., Osterheld, A. L. and Kania, D. R., *Phys. Rev. Lett.* **72**, 3029 (1994).
20. J. Denavit and D. W. Phillion, Phys. Plasmas **1**, 1971 (1994).
21. J. Dawson, P. Kaw, and B. Green, Phys. Fluids **12**, 875 (1969); J. Lindl, *Inertial Confinement Fusion* (Springer-Verlag, New York, 1998), chapter 8 and 11.
22. D. E. Post, *et al.*, At. Data Nucl. Data Tables **20**, 397 (1977).